

CMS SEARCHES IN 2010*

PIOTR ZALEWSKI

on behalf of the CMS Collaboration

The Andrzej Soltan Institute for Nuclear Studies
Hoża 69, 00-681 Warsaw, Poland*(Received April 29, 2011)*

In 2010 the CMS experiment has collected about 40/pb of proton–proton collision data at $\sqrt{s} = 7$ TeV. This allowed us to perform several searches for physics beyond Standard Model. No significant excess has been found in any of these. As a result, limits extending previous experimental constraints has been set. Some of them are the most stringent to date. Representative subset of these searches is presented.

DOI:10.5506/APhysPolB.42.1699

PACS numbers: 14.80.Ly

1. Introduction

Thanks to excellent performance of the LHC Collider and the CMS Detector [1] about 40 pb⁻¹ of proton–proton collisions at $\sqrt{s} = 7$ TeV were registered during 2010. Due to almost exponentially increasing instant luminosity the majority of this statistics were recorded at the end of the year. However, efficient analysis chains allowed to perform and approve results based on almost full statistics. For some, even a subset of data was sufficient to explore new regions of beyond Standard Model physics. Unfortunately no hint for this new physics was found. All searches performed by CMS Collaboration are as model independent as possible. They are based on almost all accessible final topologies starting from different aspects of (i) dijets systems: search for resonances [2], search for quark compositeness [3] and [4], (ii) multi object events: search for microscopic black holes [5] (see Sec. 4), (iii) dilepton plus jets: search for leptoquarks [6] and [7] (see Sec. 5), (iv) dilepton resonances [8], (v) diphoton final states: search for large extra dimensions [9], search for supersymmetry [10], (vi) jets plus missing

* Presented at the Cracow Epiphany Conference on the First Year of the LHC, Cracow, Poland, January 10–12, 2011.

transverse energy: search for supersymmetry [11] (see Sec. 2), (vii) leptons plus missing transverse energy: search for supersymmetry with opposite sign dileptons [12] (see Sec. 3), search for W' [13] and [14], search for bottom like quarks [15], (plus some not yet published analyzes which use leptonic signatures) ending at (viii) heavy stable charge particles escaping from the detector [16] and stopping in it [17] (see Sec. 6).

All analyzes use data driven techniques to estimate yields of expected SM backgrounds. In the following some of these analyzes are shortly presented.

2. Multi-jet and missing transverse energy signature

Missing energy is one of the most characteristic signatures of supersymmetry. However, it is also regarded as one suffering the most from huge QCD background due to mismeasurement of jets energies. The analysis [11] applies technique described in the Ref. [18] based on a robust dijet technique, first described in Ref. [19] extended to include multi-jet event topologies. The idea is based on a use of a kinematic variable discriminating events with true missing transverse energy from mismeasured ones without relying on purely calorimetric measurements which are susceptible to noise and non beam backgrounds.

This robust analysis technique is based on α_T variable, which is easy to define for a dijet system

$$\alpha_T = E_T^{j2}/M_T,$$

where E_T^{j2} is transverse energy of the second jet, whereas

$$M_T = \sqrt{H_T^2 - (H_T^{\text{miss}})^2}$$

is defined using scalar sum H_T and vector sum H_T^{miss} of transverse jet energies.

Multi-jet systems are reduced to two pseudo-jets, by combining jets in a way to minimize the difference between scalar sums of transverse energy of jets forming each pseudo-jet.

For ideally measured event without missing energy $\alpha_T = 0.5$. It could be seen in Fig. 1, that QCD background indeed peaks at that value for both dijet and multi-jet topologies, whereas significant part of the signal extends to the higher values of α_T , what allows to select out QCD background very efficiently.

The data sample used in the analysis was recorded with a trigger requirement $H_T^{\text{trigger}} > 150$ GeV. The jets were clustered offline by the anti- k_T algorithm with size parameter of 0.5. Only jets with $E_T > 50$ GeV, $|\eta| < 3$ and passing jet identification criteria [21]. The pseudorapidity of the jet

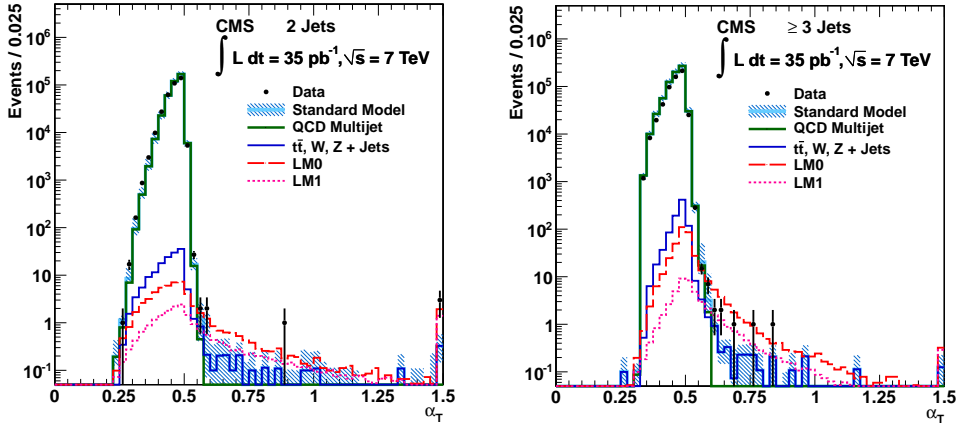


Fig. 1. Distribution of α_T for dijet (left) and multi-jet (right) events for data, SM MC background and benchmark signal MC.

with the highest E_T was required to be within $|\eta| < 2.5$ and transverse energy of the two leading jets to be above 100 GeV. Events with jets passing E_T threshold but failing η or identification criteria were vetoed. Similarly, events with isolated leptons ($p_T > 10$ GeV) or photons ($p_T > 25$ GeV) were rejected. Also events with false missing energy due to masked regions of the electromagnetic calorimeter ECAL or with large ratio $H_T^{\text{miss}}/E_T^{\text{calo}} > 1.25$ (signaling missing energy due to jets failing E_T criterion) were eliminated. Final selection was done by requiring $H_T > 350$ GeV and $\alpha_T > 0.55$ yielding 13 events in data corresponding to an integrated luminosity of 35/pb.

The SM backgrounds were evaluated with independent data control samples. First, from the lower H_T regions in data, a prediction for the total (inclusive) SM background of $9.4_{-4.0}^{+4.8}(\text{stat.}) \pm 1.0(\text{syst.})$ in the signal region was obtained. This method is illustrated in Fig. 2 where evolution of the ratio R_{α_T} of the number of events passing α_T cut to the number of events failing this cut is shown as a function of H_T for cut values of 0.51 (circles) and 0.55 (triangles). It could be seen that $R_{0.55}$ is already flat (in contrast to $R_{0.51}$) which could be attributed to the absence of non-genuine missing energy events in its numerator and allows to estimate event yields in the signal region. Electroweak (genuine missing energy) background, which dominates in the signal region was also evaluated exclusively using $W \rightarrow \mu\nu + \text{jets}$ and $\gamma + \text{jets}$ control samples to be $10.5_{-2.5}^{+3.6}$ events in agreement with the inclusive estimate and with 13 events observed in the data. Since no statistically significant excess of signal events was found the search allows to set limits. An interpretation of the search in the context of the CMMSM is shown in Fig. 3. The area below the solid (red) curve is excluded by this measurement at 95% C.L. (NLO). Exclusion limits obtained from previous experiments

are presented as filled areas in the plot. Grey lines correspond to constant squark and gluino masses. The plot also shows the two benchmark points LM0 and LM1 for comparison.

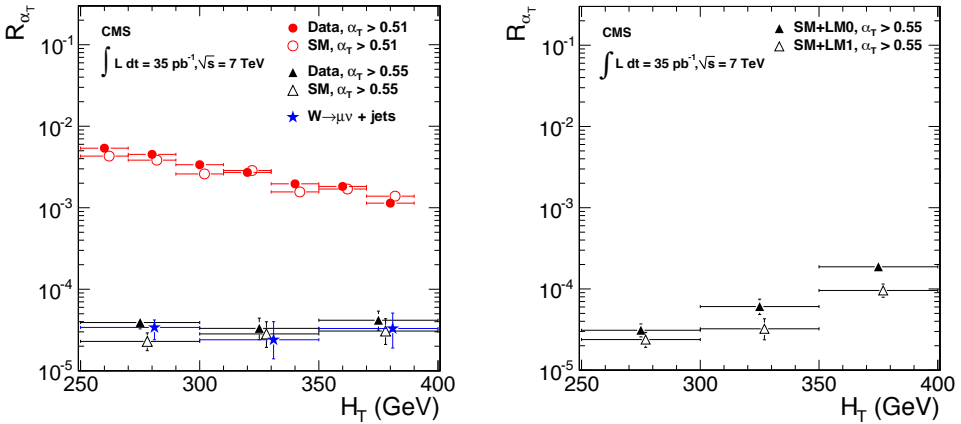


Fig. 2. Evolution of the ratio R_{α_T} as a function of H_T calculated with two α_T thresholds for: data, SM MC background and $W \rightarrow \mu\nu + \text{jets}$ control sample (left); SM MC plus benchmark signals MC (right).

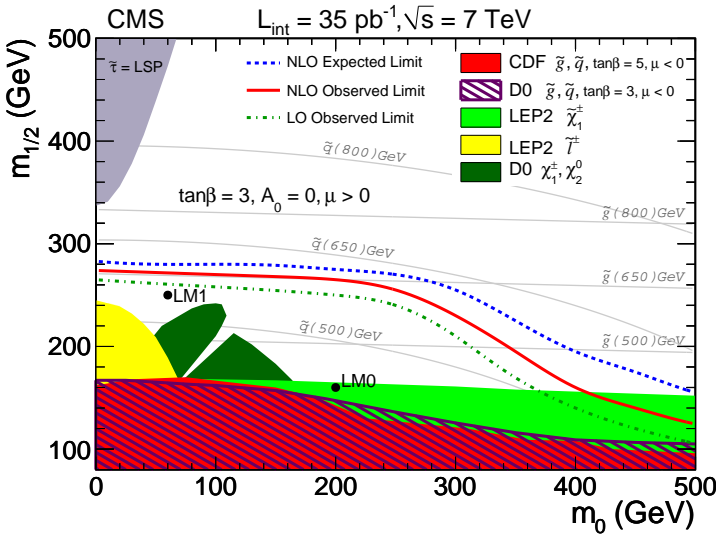


Fig. 3. The observed 95% C.L. exclusion in the CMSSM for the jets plus missing energy search.

3. Opposite-sign dilepton signature

Several BSM models predict not only multijet and missing transverse energy signature but also presence of a high transverse momentum (p_T) leptons in the final state. Publication [12] describes search for pairs of high p_T leptons accompanied by significant imbalanced (E_T^{miss}) hadronic activity. The search was model independent but CMSSM benchmark points LM0 and LM1 were used for illustration.

Preselection was based on the dilepton channel of the $t\bar{t}$ cross-section measurement [20]. Two opposite-sign, isolated leptons (electrons and muons) with transverse momentum exceeding 20 GeV/ c (first) and 10 GeV/ c (second) were required. If more than two leptons were present in the event, these with the highest p_T were chosen. Same flavor pairs with invariant mass in the vicinity of Z^0 (76–106 GeV/ c^2) or below 10 GeV/ c^2 were excluded. Only events registered due to single-lepton or double-lepton triggers were taken into account.

The presence of at least two jets with $p_T > 30$ GeV/ c and $|\eta| < 2.5$, separated by $\Delta R > 0.4$ from selected leptons were required, as well as $H_T > 100$ GeV and $E_T^{\text{miss}} > 50$ GeV (for details of the jet reconstruction, H_T and E_T^{miss} definitions see [12]).

Figure 4 shows data-simulation comparison for several kinematic variables. Data agrees well with the SM MC prediction which is dominated by $t\bar{t}$ contribution. To uncover signal an additional selection $H_T > 300$ GeV and $y = E_T^{\text{miss}}/\sqrt{H_T} > 8.5\sqrt{\text{GeV}}$ were applied. As can be seen in Fig. 5 variables y and H_T are almost uncorrelated in the SM MC (correlation coefficient $\sim 5\%$). Figure 5 shows also four ABCD regions used to estimate expected number of background events in the signal region $N_D = N_A \times N_C/N_B$ (Table I). Second, independent method used to predict number of background events (called $p_T(\ell\ell)$) was based on the idea that in the dilepton $t\bar{t}$ events p_T of charged leptons and neutrinos are correlated which allowed to model y distribution using p_T of the lepton pair. The ABCD method predicted $1.3 \pm 0.8(\text{stat.}) \pm 0.3(\text{syst.})$, the $p_T(\ell\ell)$ method predicted $2.1 \pm 2.1(\text{stat.}) \pm 0.6(\text{syst.})$, whereas one event was observed in the data. Both data driven methods agreed with each other and with Monte Carlo estimate (Table I) so expected number of background events was estimated as an error-weighted average of data driven methods to be 14 ± 0.8 in good agreement with the observed signal yield. Using this background prediction the number of non-SM events at 95% confidence level could be determined to be 4.0, which rules out two benchmark points LM0 (LM1) for which number of expected signal events is 8.6 ± 1.6 (3.6 ± 0.5). Interpretation of this result in the context of the CMSSM model is shown in Fig. 6. Exclusions are less stringent than in Fig. 3, but are complementary from a model independent interpretation point of view.

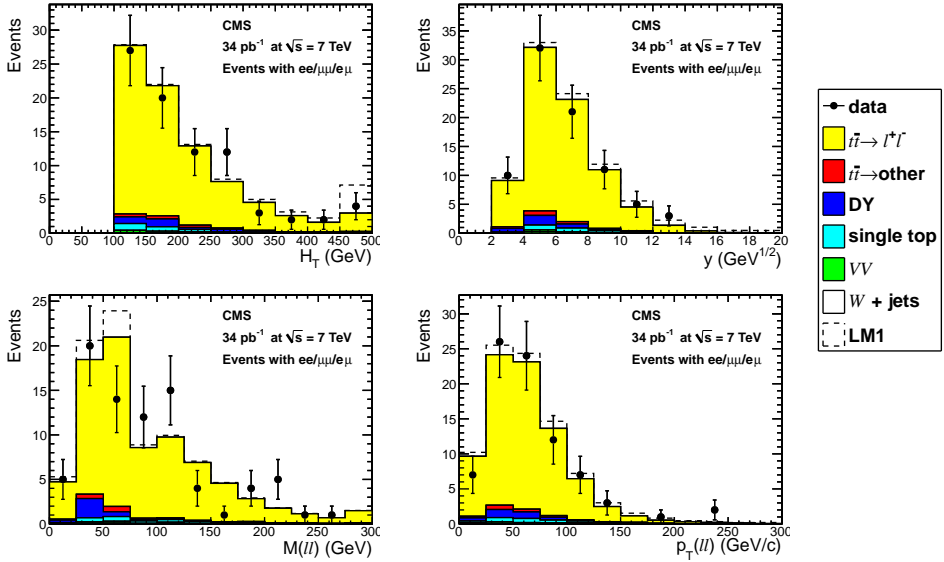


Fig. 4. Distributions of H_T , $y = E_T^{\text{miss}}/\sqrt{H_T}$, $M(\ell\ell)$ (mass of the lepton system) and $p_T(\ell\ell)$ (transverse momentum of the lepton system). The last bin contains overflow.

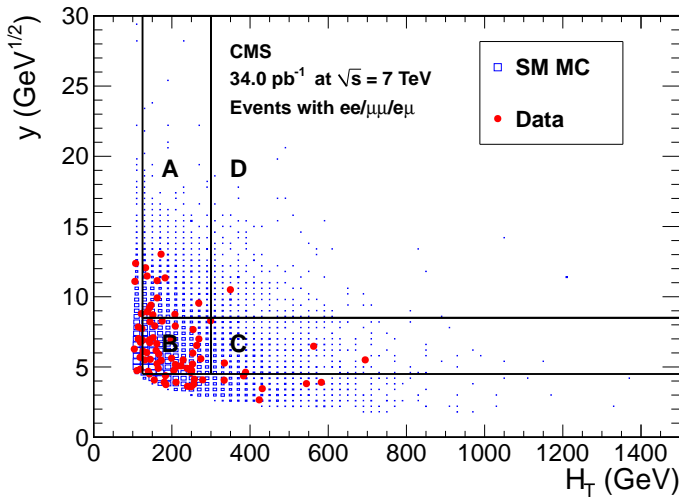


Fig. 5. Distribution of y versus H_T with depicted ABCD regions.

TABLE I

Data yields in the four ABCD regions, as well as predicted yield in the signal region D. The quoted uncertainties are statistical only.

Sample	N_A	N_B	N_C	N_D	$N_A \times N_C/N_B$
$tt \rightarrow l^+l^-$	8.44 ± 0.18	32.83 ± 0.35	4.78 ± 0.14	1.07 ± 0.06	1.23 ± 0.05
$tt \rightarrow \text{other}$	0.12 ± 0.02	0.78 ± 0.05	0.16 ± 0.02	0.02 ± 0.01	0.02 ± 0.01
Drell-Yan	0.17 ± 0.08	1.18 ± 0.22	0.04 ± 0.04	0.12 ± 0.07	0.01 ± 0.01
$W^\pm + \text{jet}$	0.00 ± 0.00	0.09 ± 0.09	0.00 ± 0.00	0.00 ± 0.00	0.00 ± 0.00
W^+W^-	0.11 ± 0.01	0.29 ± 0.02	0.02 ± 0.01	0.03 ± 0.01	0.01 ± 0.00
$W^\pm Z$	0.01 ± 0.00	0.04 ± 0.00	0.00 ± 0.00	0.00 ± 0.00	0.00 ± 0.00
ZZ	0.01 ± 0.00	0.02 ± 0.00	0.00 ± 0.00	0.00 ± 0.00	0.00 ± 0.00
Single top	0.29 ± 0.01	1.04 ± 0.03	0.04 ± 0.01	0.01 ± 0.00	0.01 ± 0.00
Total SM MC	9.14 ± 0.20	36.26 ± 0.43	5.05 ± 0.14	1.27 ± 0.10	1.27 ± 0.05
Data	12	37	4	1	1.30 ± 0.78
LM0	4.04 ± 0.19	4.45 ± 0.20	13.92 ± 0.36	8.63 ± 0.27	12.63 ± 0.88
LM1	0.52 ± 0.02	0.26 ± 0.02	1.64 ± 0.04	3.56 ± 0.06	3.33 ± 0.27

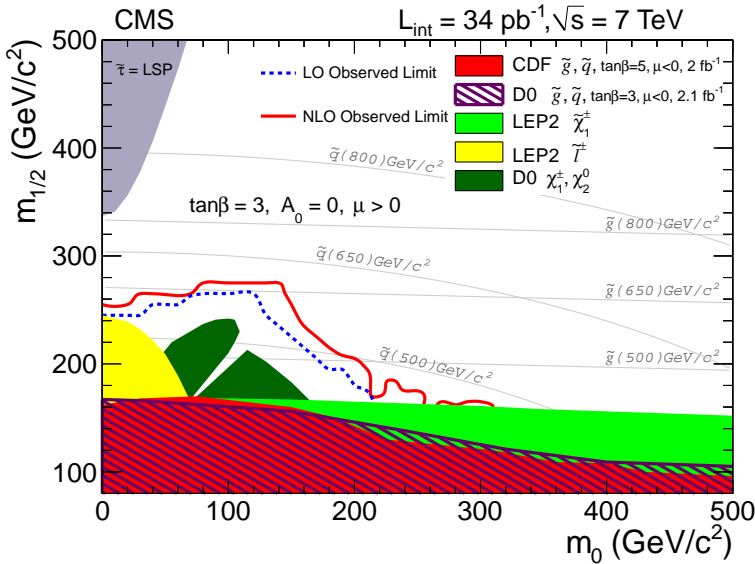


Fig. 6. The observed 95% C.L. exclusion in the CMSSM for the opposite-sign dilepton plus jets plus missing energy search.

4. Search for microscopic black holes

The possibility of production of microscopic black holes in particle collisions has been predicted in models with low scale gravity. The lowering of the scale is achieved by adding extra spatial dimensions to the SM, which are compactified. While all the SM particles are contained within a 3D membrane embedded in the multidimensional bulk space, gravity permeates the entire space. As a result, gravitational interaction is diluted. If the true Planck scale M_D is in the 1 TeV range, parton collisions with energy exceeding M_D , may collapse in a microscopic black hole. Cross-section for the microscopic black hole production is proportional to the Schwarzschild radius squared. Once produced, the microscopic black hole evaporates almost instantaneously by emitting energetic particles.

The microscopic black holes produced at the LHC would be distinguished by high multiplicity, democratic, and highly isotropic decays with the final-state particles carrying hundreds of GeV of energy. Most of these particles would be reconstructed as jets of hadrons.

The data were recorded with dedicated trigger on total jet activity H_T^{trigger} which was fully efficient for a selection based on total transverse energy S_T . The variable S_T was defined as a scalar sum of the E_T of the N individual reconstructed objects: jets, electrons, photons, and muons. Only objects with $E_T > 50$ GeV were included in the sum. Further, the missing transverse energy in the event was added to S_T , if $E_T^{\text{miss}} > 50$ GeV (without increasing object count N).

The main background to black hole signals arises from QCD multijet events. Additional backgrounds are negligible at large values of S_T and contribute less than 1% to the total background after the final selection. The dominant multijet background can only be estimated reliably from data. For QCD events, S_T is almost completely determined by the hard parton scattering process. Further splitting of the jets does not change the S_T value considerably. Consequently, the shape of the S_T distribution is expected to be independent of the event multiplicity N , as long as S_T is sufficiently large. The shape of the S_T distributions were fitted between 600 and 1100 GeV for multiplicities $N = 2$ and $N = 3$ (Fig. 7). The same parametrization was applied to higher multiplicities (normalized between 1000 and 1100 GeV, where no signal was expected).

The distribution for multiplicities $N \geq 5$ is shown in the left part of Fig. 8. No excess of data was seen what allowed to set upper limits on microscopic black holes production cross-section and mass for several theoretical models (Fig. 9).

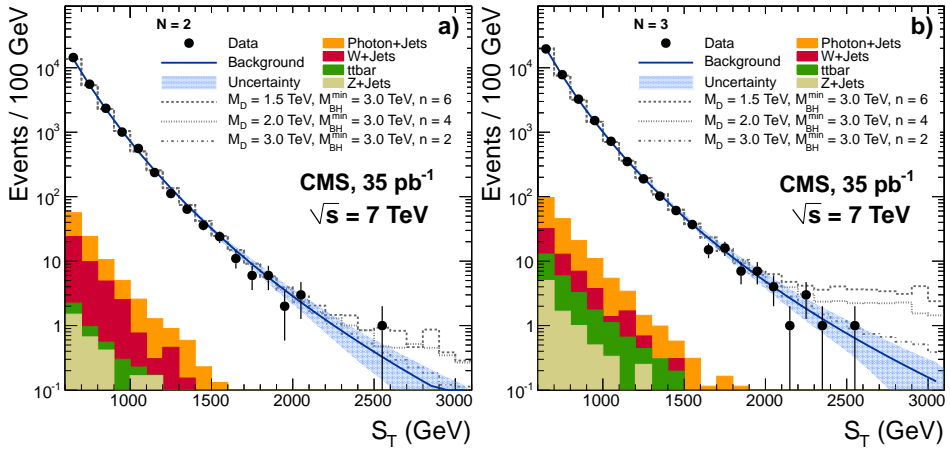


Fig. 7. Total transverse energy S_T , for events with the multiplicities of (a) $N = 2$, and (b) $N = 3$ objects in the final state. Data are depicted as solid circles with error bars; the shaded band is the background prediction obtained from data (solid line) with its uncertainty. Non-multijet backgrounds are shown as colored histograms. Also shown is the predicted black hole signal for three different parameter sets.

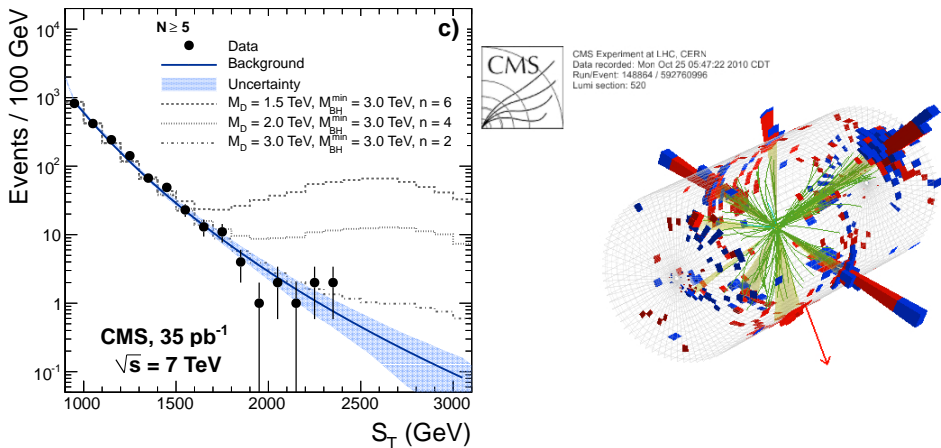


Fig. 8. Left: Total transverse energy S_T , for events with multiplicities $N \geq 5$ objects in the final state. Right: High multiplicity event with large S_T .

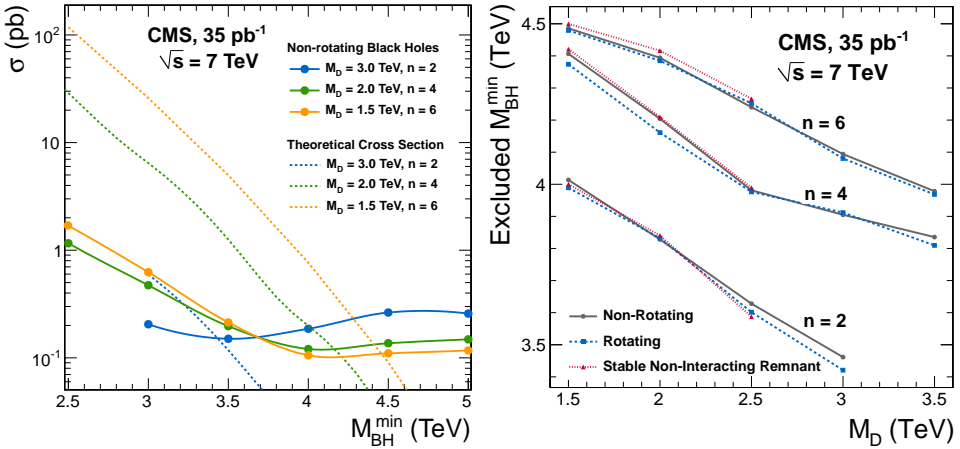


Fig. 9. Left: The 95% confidence level upper limits on the black hole production cross-section (solid lines) and three theoretical predictions for the cross-section (dotted lines), as a function of the black hole mass. Right: The 95% confidence level limits on the black hole mass as a function of the multidimensional Planck scale M_D for several benchmark scenarios. The area below each curve is excluded by the search.

5. Search for leptoquarks

Some well motivated theories of physics beyond the SM, including grand unified theories, composite models, technicolor, and superstring inspired E6 models, postulate the existence of a symmetry, beyond that of the SM, relating quarks and leptons and implying the existence of new bosons, called leptoquarks (LQ). A LQ carries color, has fractional electric charge, can have spin 0 (scalar) or spin 1 (vector), and couples to a lepton and a quark with coupling strength λ .

A LQ would decay to a charged lepton and a quark, with an unknown branching fraction β^2 , or a neutrino and a quark, with branching fraction $1 - \beta^2$. At LHC LQs are predominantly produced in pairs via gluon–gluon fusion and quark–antiquark annihilation with a cross-section that depends on the strong coupling constant but is nearly independent of λ .

A search for pair production of first-generation scalar leptoquarks was performed in the final state containing two electrons and two jets [6], whereas a search for pair production of second-generation scalar leptoquarks in the final state with two muons and two jets [7]. Both analyzes were very similar. The distributions of dilepton mass and total energy S_T are shown in Fig. 10 for first- and 11 second-generation leptoquarks.

The number of collision events, passing a selection optimized for exclusion of the LQ hypothesis, is in good agreement with the predictions for the SM background processes. A Bayesian approach that includes the treatment of the systematic uncertainties as nuisance parameters has been used to set an upper limit on the first-generation (Fig. 12) and second-generation (Fig. 13) LQ cross-sections.

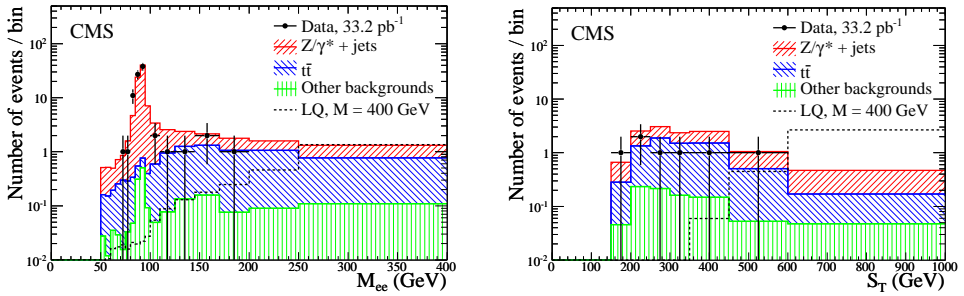


Fig. 10. Left: The M_{ee} distribution for events that have passed the pre-selection requirements. Right: The S_T distribution for events that have passed the pre-selection requirement, except the pre-selection requirement on S_T itself ($S_T > 250$ GeV), and have $M_{ee} > 125$ GeV. The MC distributions for the signal ($\beta = 1$) and the contributing backgrounds are shown. All background histograms are cumulative.

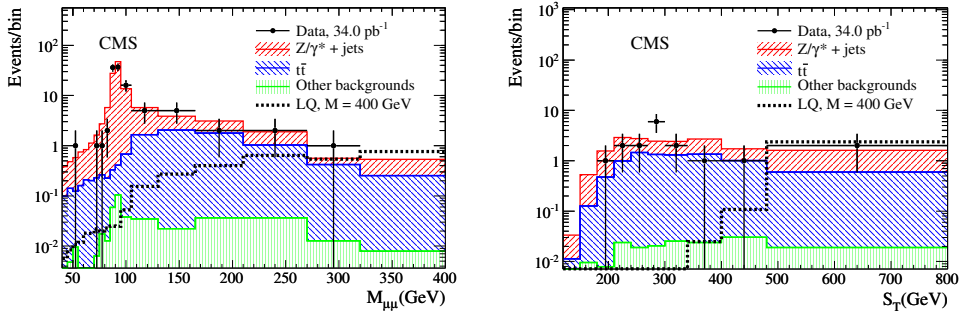


Fig. 11. Left: The distribution of $M_{\mu\mu}$ after requiring at least two muons and at least two jets with $p_T > 30$ GeV and $S_T > 250$ GeV. Right: The distribution of S_T after requiring at least two muons and at least two jets with $p_T > 30$ GeV and $M_{\mu\mu} > 115$ GeV. The $Z/\gamma^* \rightarrow \mu\mu + \text{jets}$ contribution is rescaled by the factor 1.28. Other backgrounds correspond to VV , $W + \text{jets}$, and multijet processes. Uncertainties are statistical.

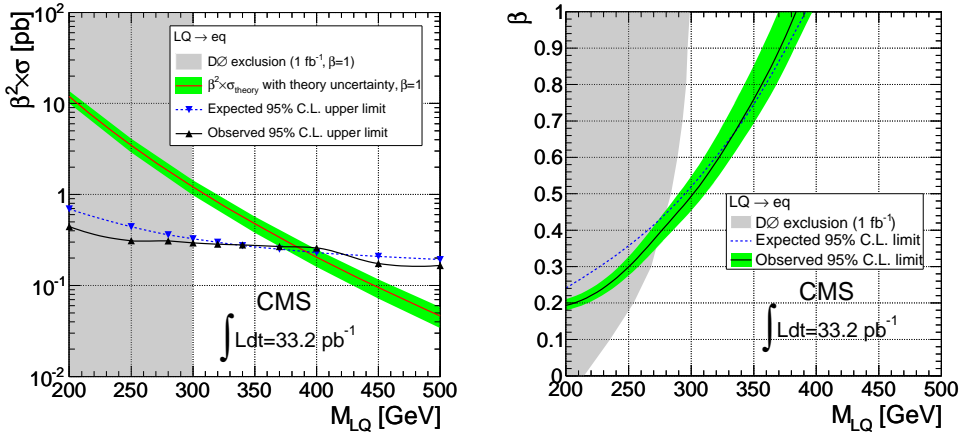


Fig. 12. Left: The expected and observed upper limit at 95% C.L. on the LQ pair production cross-section times β^2 as a function of the LQ mass. The systematic uncertainties are included in the calculation. The shaded region is excluded by the current D0 limit for $\beta = 1$. The σ_{theory} curve and its band represent, respectively, the theoretical LQ pair production cross-section and its uncertainties. Right: Minimum β for a 95% C.L. exclusion of the LQ hypothesis as a function of LQ mass. The observed (expected) exclusion curve is obtained using the observed (expected) upper limit and the central value of the theoretical LQ pair production cross-section. The band around the observed exclusion curve is obtained by considering the observed upper limit while taking into account the uncertainties on the theoretical cross-section. The shaded region is excluded by the current D0 limits, which combines results from searches in the two electron, electron–neutrino, and two neutrino channels.

By comparing this upper limit to a theoretical calculation of the LQ pair production cross-section, the existence of first-generation scalar LQ with masses below 384 GeV for $\beta = 1$ has been excluded at 95% C.L., with a corresponding cross-section limit of 0.267 pb. The lower limits on the LQ mass set for values of β larger than about 0.4 are the most restrictive direct limits to date.

At 95% C.L., the pair production of second-generation scalar leptoquarks with masses below 394 GeV has been excluded for $\beta = 1$, where β is the leptoquark branching fraction into a muon and a quark. This is the most stringent limit to date on the existence of second-generation scalar leptoquarks.

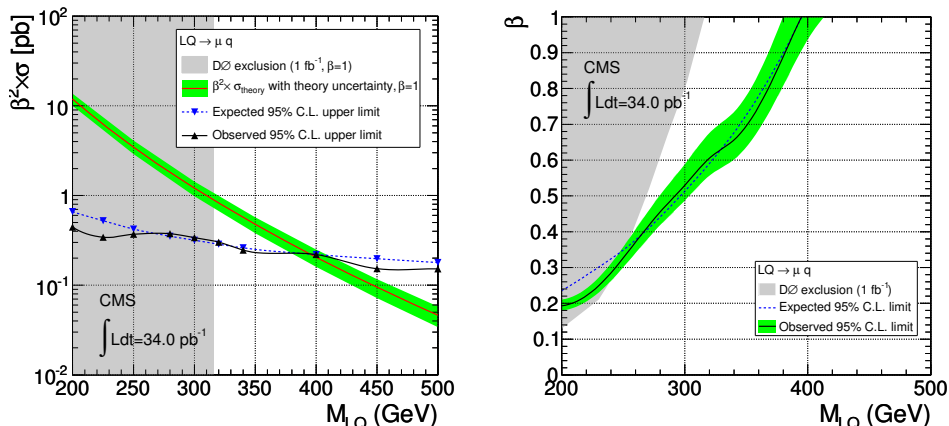


Fig. 13. Left: The expected and observed 95% C.L. upper limit on the scalar leptoquark pair production cross-section multiplied by β^2 as a function of the LQ mass, together with the NLO theoretical cross-section curve. The shaded band on the theoretical values includes CTEQ6.6 PDF uncertainties and the error on the leptoquark production cross-section due to renormalization and factorization scale variation by a factor of two. The shaded region is excluded by the current D0 limits. Right: The minimum β for 95% C.L. exclusion of the leptoquark hypothesis as a function of leptoquark mass. The observed limit and corresponding uncertainty band is obtained by considering the observed upper limit and theoretical branching ratio and its uncertainty in the left-hand figure. Note: The shaded area excluded by the D0 experiment was determined with combined information from the decay channel with two muons and two jets and the decay channel with one muon, missing transverse energy, and two jets.

6. Search for stopped gluinos during beam-off periods

If long-lived gluinos were produced at the LHC, they would hadronize into so called R-hadrons some of which would be charged, while others would be neutral. Those that were charged would lose energy via ionization as they traverse the CMS detector. For slow R-hadrons, this energy loss would be sufficient to bring a significant fraction of the produced particles to rest inside the CMS detector volume. In Fig. 14 the distributions of gluino stopping points inside CMS are shown.

These stopped R-hadrons may decay seconds, days, or even weeks later, resulting in a jet like energy deposit in the CMS calorimeter. These decays will be out of time with respect to LHC collisions and may well occur at times when there are no collisions in CMS.

The 7 TeV center-of-mass pp collision data analyzed in this analysis [17] were recorded by CMS between April and October 2010. We divide these data into two samples: the first corresponds to 95 hours of trigger live-

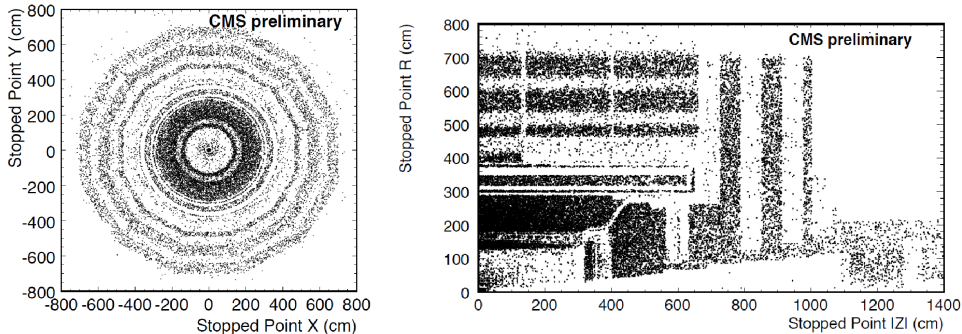


Fig. 14. R-hadron stopping points for $m_{\tilde{g}} = 300$ GeV.

time during LHC fills, in which the instantaneous luminosity was $27 \times 10^{27} \text{cm}^{-2} \text{s}^{-1}$. This period was used as a control sample to estimate the background rate. Because these data were recorded at relatively low instantaneous luminosity, there is negligible risk that a stopped-particle signal is present in this sample. The second sample, where a search for the presence of a stopped-particle signal were performed, corresponds to 62 hours of trigger live-time during which data, corresponding to an integrated luminosity of 10/pb, were recorded by CMS with a peak instantaneous luminosity of $10^{32} \text{cm}^{-2} \text{s}^{-1}$. In producing these data, the LHC was filled with up to 312 proton bunches per beam (out of a maximum of 2808). A dedicated trigger was employed to search for decays of particles at times when there are no collisions. Information from the beam position and timing (BPTX) monitors were used to identify gaps between the proton bunches that comprise the LHC beam. The BPTX monitors were positioned 175 m from the center of CMS on either side of the CMS interaction region and produce a signal when an LHC proton bunch passes the monitor. Even though the R-hadron decay does not produce a true jet, the resultant energy deposition is sufficiently jet like that a jet trigger is reasonably efficient. We therefore require a jet trigger together with the condition that a coincidence of signals from both BPTX did not occur, ensuring that the trigger will not fire on jets produced from pp collisions.

After the selection [17] a counting experiment and a time-profile analysis on the remaining data were performed. For the counting experiment gluino lifetime hypotheses from 75 ns to 10^6 s were taken into account. In the search sample no significant excess above expected background was observed for any lifetime hypothesis. In the absence of any discernible signal 95% confidence level (C.L.) limits were set over 13 orders of magnitude in gluino lifetime (Figs. 15 and 16).

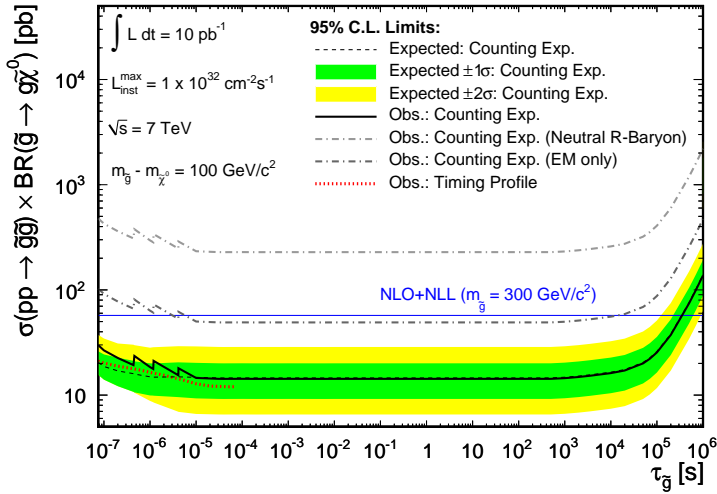


Fig. 15. Expected and observed 95% C.L. limits on gluino pair production cross-section times branching fraction using the “cloud model” of R-hadron interactions as a function of gluino lifetime from both the counting experiment and the time-profile analysis. Observed 95% C.L. limits on the gluino cross-section for alternative R-hadron interaction models are also presented.

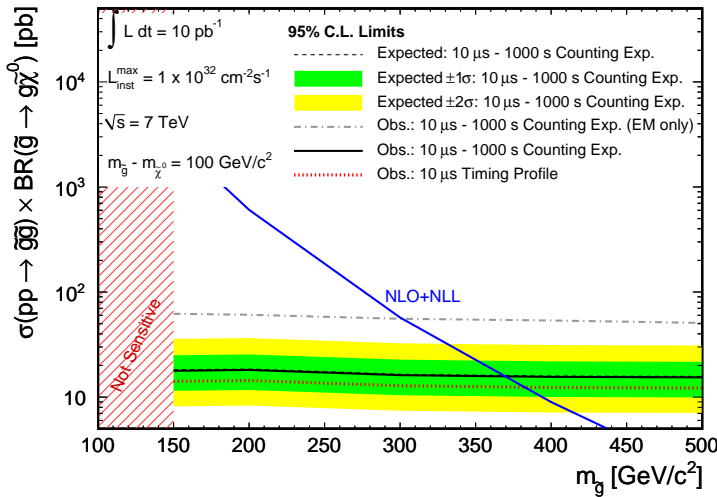


Fig. 16. 95% C.L. limits on gluino pair production cross-section times branching fraction as a function of gluino mass assuming the “cloud model” of R-hadron interactions (solid line) and EM interactions only (dot-dashed line). The gluino–neutralino mass difference is maintained at 100 GeV/c²; results are only presented for neutralino mass above 50 GeV/c².

For gluino lifetimes from 75 ns to $100\mu\text{s}$ a time-profile analysis were also performed because the signal and background have very different time profiles (Fig. 17). The results are also shown in Figs. 15 and 16.

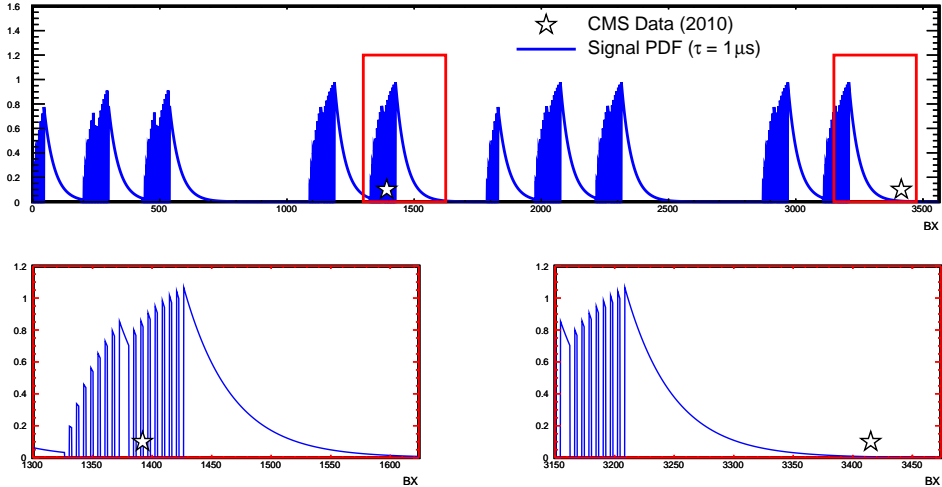


Fig. 17. The top panel shows the in-orbit positions of 2 observed events in the subset of our data that was recorded during an LHC fill with 140 colliding bunches. The decay profile for a $1\mu\text{s}$ lifetime hypothesis is overlaid. The bottom panels are zoomed views of the boxed regions around the 2 events in the top panel so that the exponential decay shape of the signal hypothesis can be seen.

These results extend existing limits from the D0 Collaboration on both gluino lifetime and gluino mass. These limits are the most restrictive to date.

7. Summary

Representative subset of recent searches for beyond Standard Model using CMS detector at LHC was presented. All analyzes were based on data collected during 2010. No hint for new physics were found. At the end of March 2011 the statistic is almost doubled and it should increase by more than an order of magnitude till end of the year and even more in the 2012. With each triggered event we are closer and closer to the discovery we are waiting for. We do our best to ensure that topology in which new physics is to show up is in our trigger and analysis menu.

I would like to thank organizers of the Cracow Epiphany Conference for invitation and hospitality. This work was supported in part by the Polish Ministry of Science and Higher Education grants N N202 167440 (1674/B/H03/2011/40), N N202 230337 and 666/N-CERN/2010/0.

REFERENCES

- [1] [CMS Collaboration], *JINST* **3**, S08004 (2008).
- [2] [CMS Collaboration], *Phys. Rev. Lett.* **105**, 211801 (2010).
- [3] [CMS Collaboration], *Phys. Rev. Lett.* **105**, 262001 (2010).
- [4] [CMS Collaboration], *Phys. Rev. Lett.* **106**, 201804 (2011) [[arXiv:1102.2020v1](#) [[hep-ex](#)]].
- [5] [CMS Collaboration], *Phys. Lett.* **B697**, 434 (2011).
- [6] [CMS Collaboration], *Phys. Rev. Lett.* **106**, 201802 (2011) [[arXiv:1012.4031v1](#) [[hep-ex](#)]].
- [7] [CMS Collaboration], *Phys. Rev. Lett.* **106**, 201803 (2011) [[arXiv:1012.4033v1](#) [[hep-ex](#)]].
- [8] [CMS Collaboration], [arXiv:1103.0981v2](#) [[hep-ex](#)].
- [9] [CMS Collaboration], [arXiv:1103.4279v1](#) [[hep-ex](#)].
- [10] [CMS Collaboration], [arXiv:1103.0953v2](#) [[hep-ex](#)].
- [11] [CMS Collaboration], *Phys. Lett.* **B698**, 196 (2011).
- [12] [CMS Collaboration], [arXiv:1103.1348v1](#) [[hep-ex](#)].
- [13] [CMS Collaboration], [arXiv:1012.5945v2](#) [[hep-ex](#)].
- [14] [CMS Collaboration], [arXiv:1103.0030v1](#) [[hep-ex](#)].
- [15] [CMS Collaboration], [arXiv:1102.4746v1](#) [[hep-ex](#)].
- [16] [CMS Collaboration], [arXiv:1101.1645v1](#) [[hep-ex](#)].
- [17] [CMS Collaboration], *Phys. Rev. Lett.* **106**, 011801 (2010).
- [18] [CMS Collaboration], Search Strategy for Exclusive Multi-jet Events from Supersymmetry at CMS, CMS PAS SUS-09-001.
- [19] L. Randall, D. Tucker-Smith, *Phys. Rev. Lett.* **101**, 221803 (2008).
- [20] [CMS Collaboration], *Phys. Lett.* **B695**, 424 (2011).
- [21] [CMS Collaboration], Calorimeter Jet Quality Criteria for the First CMS Collision Data, CMS Physics Analysis Summary JME-09-008, 2009.